

Flat bands, non-trivial band topology and electronic nematicity in layered kagome-lattice RbTi_3Bi_5

Zhicheng Jiang,^{1,2,*} Zhengtai Liu,^{1,†} Haiyang Ma,^{3,4,*} Wei Xia,^{3,4,*} Zhonghao Liu,^{1,2} Jishan Liu,^{1,2} Soohyun Cho,¹ Yichen Yang,^{1,2} Jianyang Ding,^{1,2} Jiayu Liu,^{1,2} Zhe Huang,^{1,2} Yuxi Qiao,^{1,2} Jiajia Shen,^{1,2} Wenchuan Jing,^{1,2} Xiangqi Liu,^{3,4} Jianpeng Liu,^{3,4,‡} Yanfeng Guo,^{3,4,§} and Dawei Shen^{1,2,¶}

¹State Key Laboratory of Functional Materials for Informatics,
Shanghai Institute of Microsystem and Information Technology,
Chinese Academy of Sciences, Shanghai 200050, China

²Center of Materials Science and Optoelectronics Engineering,
University of Chinese Academy of Sciences, Beijing 100049, China

³School of Physical Science and Technology, ShanghaiTech University, Shanghai 201210, China

⁴ShanghaiTech Laboratory for Topological Physics, ShanghaiTech University, Shanghai 201210, China

Layered kagome-lattice materials with $3d$ transition metals provide a fertile playground for studies on geometry frustration, band topology and other novel ordered states. A representative class of materials AV_3Sb_5 ($A=\text{K}, \text{Rb}, \text{Cs}$) have been proved to possess various unconventional phases such as superconductivity, non-trivial \mathbb{Z}_2 band topology, and electronic nematicity, which are intertwined with multiple interlaced charge density waves (CDW). However, the interplay among these novel states and their mechanisms are still elusive. Recently, the discovery of isostructural titanium-based single-crystals ATi_3Bi_5 ($A=\text{K}, \text{Rb}, \text{Cs}$), which demonstrate similar multiple exotic states but in the absence of the concomitant intertwined CDW, has been offering an ideal opportunity to disentangle these complex novel states in kagome-lattice. Here, we combine the high-resolution angle-resolved photoemission spectroscopy and first-principles calculations to systematically investigate the low-lying electronic structure of RbTi_3Bi_5 . For the first time, we experimentally demonstrate the coexistence of flat bands and multiple non-trivial topological states, including type-II Dirac nodal lines and non-trivial \mathbb{Z}_2 topological surface states therein. Furthermore, our findings as well provide the hint of rotation symmetry breaking in RbTi_3Bi_5 , suggesting the directionality of the electronic structure and possibility of emerging pure electronic nematicity in this new family of kagome compounds, which may provide important insights into the electronic nematic phase in correlated kagome metals.

In recent years, kagome-lattice materials containing frustrated corner-sharing triangles provide an exciting platform to investigate the interplay between electron correlations, lattice geometry and band topology [1–9]. Since electrons are localized in the unique frustrated honeycomb hexagonal structure, kagome-lattice materials simultaneously host flat bands, van Hove singularities (VHSs) and Dirac band crossings, which subsequently give rise to a series of novel quantum states depending on the band filling, such as quantum spin liquid, fractional quantum Hall states and density waves [10–15]. In particular, kagome-lattice metals have long been predicted to host unconventional chiral and spin-triplet superconductivity (SC) when the chemical potential is tuned to be close to VHSs [16–20]. Consequently, the layered kagome-lattice AV_3Sb_5 ($A=\text{K}, \text{Rb}, \text{and Cs}$), in which both the \mathbb{Z}_2 non-trivial topological band [21] and superconductivity [22–26] were discovered, rapidly sparked enormous research interests [19, 26–36]. The suggested strong-coupling superconductivity with possible triplet pairing and non-trivial band topology therein might pave the way for realizing the long-sought-after Majorana zero modes. Furthermore, more unexpected exotic ordered states discovered in AV_3Sb_5 , including unidirectional charge order, rotation symmetry breaking and

roton pair density waves, further stimulated the research interest in this family of materials because they are akin to those correlated physics in high-temperature superconductors. To date, it has been becoming one of the research frontiers, which aims to decode these ordered states and then further disentangle their interrelation.

Moreover, the canonical electronic structure with symmetry-protected flat and topological bands as well renders kagome-lattice materials a promising sandbox to explore and try out novel quantum states [37, 38]. Unfortunately, previously reported band structures have demonstrated that both flat bands and \mathbb{Z}_2 topological surface states in AV_3Sb_5 are far away from or well above the Fermi level (E_F), which consequently triggers a repulsive barrier to the interaction of flat or non-trivial topological bands with exotic ordered states in the vicinity of E_F . Recently, the discovery of new AB_3C_5 members ATi_3Bi_5 ($A=\text{Rb}, \text{Cs}$), in which V ($3d^3$) and Sb atoms are completely substituted by Ti ($3d^2$) and heavier Bi atoms, respectively, compared to AV_3Sb_5 , paves a promising way to address this issue [39, 40]. On one hand, the substantial equivalent hole doping due to the reduction of band filling effectively brings the flat bands close to E_F [41–43]; on the other hand, the stronger spin-orbital coupling (SOC) can be more likely to cause the band inversion, leading to richer topological band characteristics. Although the superconductivity therein are still in debate, there is no doubt that ATi_3Bi_5 could provide a promising playground for further exploring the interplay between topology, superconductivity and geometric frustration in kagome-lattice. Furthermore, since no evidence on the existence of CDW phase occurring

* Equal contributions

† Equal contributions; ztliu@mail.sim.ac.cn

‡ liujp@shagnhaitech.edu.cn

§ guoyf@shanghaitech.edu.cn

¶ dwshen@mail.sim.ac.cn

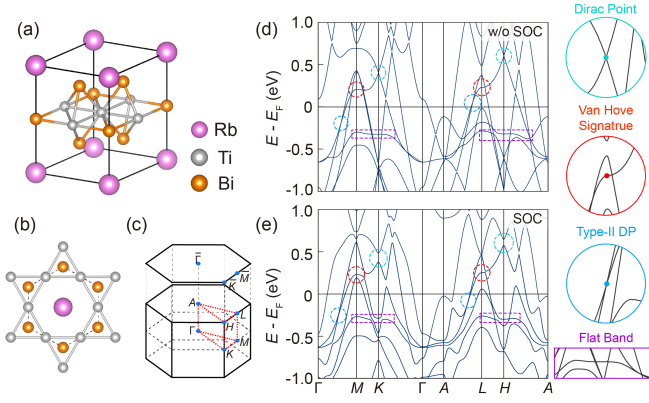


FIG. 1. (a) Crystal structure of RbTi_3Bi_5 . (b) Top view of the Ti-kagome network. (c) Bulk Brillouin zone (BZ) and projected two-dimensional BZ attached with high-symmetry points are indicated. Calculated band structure of RbTi_3Bi_5 along high-symmetry paths (d) without SOC and (e) with SOC.

in ATi_3Bi_5 have been reported, they become ideal model systems for comparison study of the electronic nematicity in kagome-lattice without the interference of translation symmetry breaking CDW as in AV_3Sb_5 .

In this work, we present the first report on the low-lying electronic structure of RbTi_3Bi_5 , one typical ATi_3Bi_5 compound, using high-resolution angle-resolved photoemission spectroscopy (ARPES) together with first-principles calculations. We reveal multiple coexisting topological states in this sibling material of AV_3Sb_5 : flat bands, type-II Dirac nodal lines and topological surface states in the vicinity of E_F . The kagome-lattice driven flat bands in RbTi_3Bi_5 are located at ~ 0.25 eV below E_F . At nearly the same binding energy, there exist a set of type-II Dirac cones, and they form type-II Dirac nodal lines along the k_z direction, which are discovered to intertwine with flat bands. Moreover, we reveal the existence of \mathbb{Z}_2 topological surface states both in the center and at the boundary of Brillouin zone. Furthermore, our autocorrelation results on RbTi_3Bi_5 and KV_3Sb_5 ARPES data suggest the anisotropic scattering along different wavevector directions, indicating a hidden nematic phase in RbTi_3Bi_5 at low temperatures. We also discuss the intercorrelation between the vanishing CDW order and VHSs in ATi_3Bi_5 .

RbTi_3Bi_5 shares the same crystal structure as AV_3Sb_5 , and it crystallizes in the space group $\text{P6}/\text{mmm}$ with lattice constants $a = 5.77$ Å and $c = 9.065$ Å [39, 40, 44, 45]. As shown in Fig. 1(a), it consists of Ti-Bi slabs, Bi honeycomb layers and alkali Rb triangle networks stacking alternately along the c axis. Here, those core two-dimensional (2D) kagome layers are composed of Ti atoms in Ti-Bi slabs [Fig. 1(b)]. The three-dimensional (3D) and projected (001) surface Brillouin zones (BZs) of RbTi_3Bi_5 are illustrated in Fig. 1(c), in which plotted black dots indicate high-symmetry momenta. More details on the sample preparation, characterization and calculations can be found in Supplementary Material (SM) [46].

Figures 1(d) and 1(e) show calculated band structures of

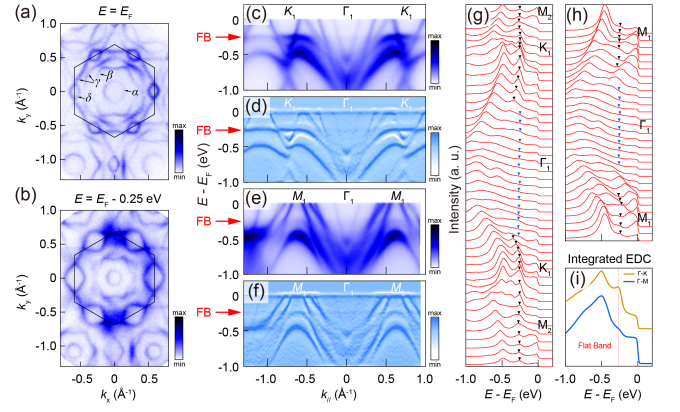


FIG. 2. (a) Fermi surface (E_F) and (b) constant energy contours at $E_F - 0.25$ eV of RbTi_3Bi_5 measured with 66 eV photons. Hexagonal surface Brillouin zones are marked with dark solid lines. (c), (e) ARPES intensity plot and (d), (f) corresponding curvature derivative plots along Γ - K - M and Γ - M high-symmetry direction, respectively. (g) EDCs of (c). (h) EDCs of (e). The flat bands around K , M and shadow flat band around Γ point are indicated by black and blue inverted triangles, respectively. (i) Integrated energy distribution curves along Γ - M (blue) and Γ - K (gold) direction. The position of flat band is marked with red dash line.

RbTi_3Bi_5 wo/w the SOC, respectively. Although the substantial SOC from Bi atoms introduces significant changes to some of bands, we can still identify typical band features of kagome-lattice, e.g., VHSs located at $\sim E_F + 0.2$ eV at M/L and Dirac points (DPs) located at $\sim E_F + 0.5$ eV at K/H , which are highlighted in the zoomed-in circles on the right. However, distinct from AV_3Sb_5 , both features are far away from E_F . In contrast, we have found pronounced flat bands, which are located just slightly below E_F (~ -0.25 eV). Furthermore, along the high-symmetry direction Γ/A - M/L and at nearly the same binding energy, we have discovered a type-II DP as well, as shown in the right enlarged blue circle.

We then experimentally searched for the predicted flat bands. Firstly, we demonstrate ARPES intensity mapping of Fermi surface taken with 66 eV photons for RbTi_3Bi_5 , as illustrated in Fig. 2(a). There exist four dispersive bands crossing E_F labeled by α to δ , forming one circle-like (α band) and one hexagonal-like (β band) electron pocket. The γ band crosses through E_F two times, which forms a hexagonal-like electron pocket around zone centre and a triangle-like hole pocket around the corner of BZ. Additionally, the δ band constitutes a rhombic-like hole pocket around the boundary of BZ. As the increase of binding energy, high density of states (DOS) appears near the K points at around $E_F - 0.25$ eV, and then disappears at higher binding energy [Fig. 2(b) and Fig. S2 in SM [46]], indicating the existence of dispersionless bands. To explore the possible dispersionless bands, we present detailed photoemission intensity images and their corresponding second derivative plots along the representative Γ - M and Γ - K directions, respectively [Figs. 2(c-f)]. As indicated by red arrows, all these data clearly show rather flat band feature at the very binding energy of 0.25 eV, which is reminiscent of the characteristic of electronic structure in kagome-lattice.

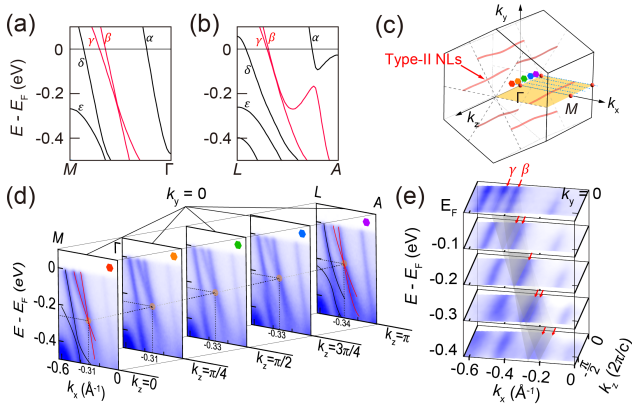


FIG. 3. Calculated bulk bands along (a) Γ - M and (b) L - A , α - ϵ mark the first to fifth band from Γ to M point, respectively. The β and γ bands forming type-II Dirac cone are highlighted by red lines. (c) Schematic of momentum locations of type-II Dirac nodal lines (NLS) and cut lines along different k_z position (blue dash lines) in the bulk BZ. (d) ARPES intensity plots cut along the Γ - M direction at selected k_z positions ($k_z = 0, \pi/4, \pi/2, 3\pi/4$ and π). Origin dots denote the position of type-II Dirac nodes. (e) The stacking constant energy k_x - k_z maps along Γ - M direction taken at selected energies (E_F to E_F -0.4 eV).

Such flat band feature can be further confirmed by both the non-dispersive peak in the energy distribution curves (EDCs) [Figs. 2(g-f)] and shoulders in the integrated EDCs [Fig. 2(i)] along $\Gamma - K$ and $\Gamma - M$, respectively. This flat band at ~ -0.25 eV is seemingly across the entire BZ, distinct from our calculation in which the flat band is absent in the regions along $\Gamma - K$ and $\Gamma - M$ as shown in Figs. 1(e-f). Note that we have identified such similar flat band feature in all ATi_3Bi_5 , as shown in SM [46]. Such a feature is especially conspicuous in KTi_3Bi_5 , in which two prominent flat bands and VHSs coincide at nearly the same binding energies (See Fig. S3 in SM [46]). It is worthy of note that such a band behavior has been as well reported in V-based kagome superconductors [21].

Distinct from AV_3Sb_5 , Ti-based kagome metals exhibit richer non-trivial band topology in the vicinity of E_F . In Figs. 3(a) and 3(b), we demonstrate the zoomed-in calculated band structure of RbTi_3Bi_5 around predicted type-II DPs. Along both the $\Gamma - M$ or $A - L$ high-symmetry directions, there exist two linear bands (four when considering the spin degeneracy caused by the combined time-reversal and spatial-inversion symmetries) which cross at a type-II DP at E_F -0.2 eV. This DP is exact and protected by both spacial-inversion and time-reversal (PT) symmetry when the SOC is ignored, and even the consideration of SOC would just introduce a tiny gap of 9 meV. In total there are six type-II DPs over the $k_x - k_y$ plane, and they all evolve into Dirac nodal lines (DNLs) along k_z since the interlayer couplings are weak. To experimentally verify these type-II DNLs, we performed a detailed photon-energy dependent ARPES measurement, in which all probing cuts were intentionally arranged to fully cover the localization of one DNL in the momentum space, as illustrated in Fig. 3(c). Through spectra along these cuts (with different

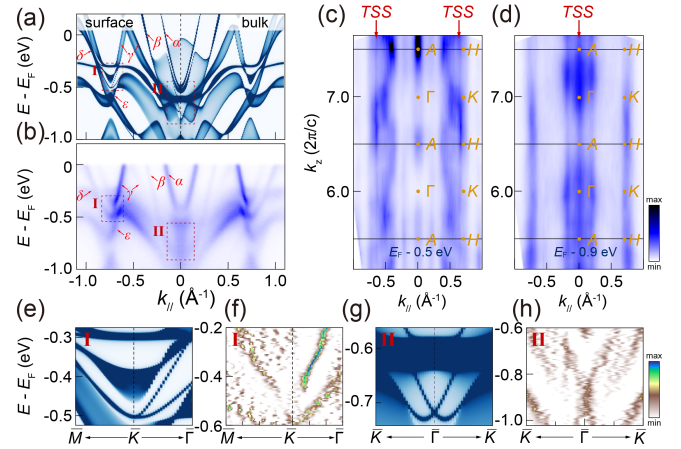


FIG. 4. (a) Calculated band structure without (left half) and with surface (right half) states. (b) The $k_{//}$ - E ARPES spectra taken along \bar{K} - $\bar{\Gamma}$ - \bar{K} direction. Large-scale constant energy k_x - k_z map along \bar{K} - $\bar{\Gamma}$ - \bar{K} direction taken at (c) E_F -0.5 eV and (d) E_F -0.9 eV. The solid lines denote the boundary of Brillouin zones. (e), (f) The zoomed-in calculated band structure \bar{K} and $\bar{\Gamma}$ point. (g), (h) The zoomed-in 2D curvature ARPES spectra taken around \bar{K} and $\bar{\Gamma}$ point.

k_z) shown in Fig. 3(d), we can distinguish a series of type-II Dirac-like band crossings, which are markedly in line with our calculation [red lines in Fig. 3(c)]. Furthermore, we plot the k_x - k_z constant-energy contours integrated within a 50 meV energy window from E_F to E_F -0.4 eV across half of the BZ in Fig. 3(e). We can discover that the β and γ bands degenerate to a single curving nodal line exactly at the binding energy of 0.2 eV, as marked by the red arrow. In this way, we can unambiguously confirm the existence of type-II DNLs in RbTi_3Bi_5 . Note that these DNLs are rather close to E_F , and they probably make significant topological contribution to transports.

Aside from DNLs, there exists a well-defined topological gap for the γ band. Since the PT symmetry is conserved in RbTi_3Bi_5 , a Fu-Kane \mathbb{Z}_2 index can be associated to the four time-reversal-invariant points [47]. We calculated their parity eigenvalues (Table S1 in SM [46]), which lead to a strong topological insulator state, similar to previous calculations [39]. Therefore, there should be non-trivial topological surface states (TSSs) in the bulk gap of RbTi_3Bi_5 . We show our calculated and experimental band structures around these TSSs in Figs. 4(a) and 4(b), respectively. Theoretically, we can indeed observe these TSSs appearing in the bulk band gap in the regions I and II, as shown in Figs. 4(a), 4(e) and 4(g). Our experimental band dispersion shows overall good agreement with the calculation. In particular, through second derivatives of photoemission intensity images [Figs. 4(f) and 4(h)], all predicted TSSs can be well resolved. We can clearly identify the characteristic split bands around \bar{K} and Rashba-like feature around $\bar{\Gamma}$ except for a small offset and renormalization of binding energy. Furthermore, our photon-energy dependent $k_{//}$ - k_z mappings around regions I [Fig. 4(c)] and II [Fig. 4(d)] confirm the surface band nature of these resolved bands. Thus, we can verify the existence of non-trivial TSSs in RbTi_3Bi_5 .

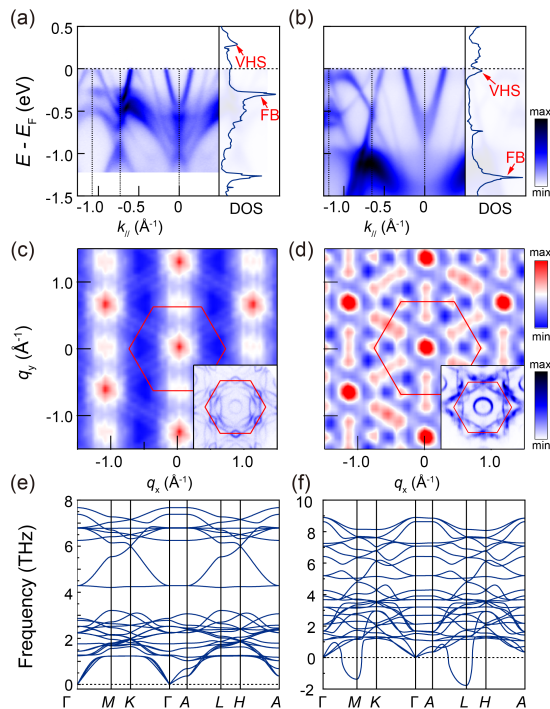


FIG. 5. ARPES intensity plot of (a) RbTi_3Bi_5 and (d) KV_3Sb_5 along $\overline{M-K-\Gamma}$ high-symmetry direction. The calculated density of states (DOS) are appended on the right side of corresponding panels; Two-dimensional joint DOS results from experimental Fermi surface of (c) RbTi_3Bi_5 and (d) KV_3Sb_5 . The insets are experimental Fermi surfaces; Calculated phonon spectrum along a high-symmetry path of (e) RbTi_3Bi_5 and (f) KV_3Sb_5 .

One pivotal feature of ATi_3Bi_5 is the absence of CDW, which is as well regarded as one major advantage over V-based kagome metals in studying the electronic nematicity in kagome lattices [48]. Accordingly, in our photoemission data we did not observe any sign of energy gap or band folding even at the lowest temperature we can achieve [Fig. 5(a) and Fig. S6 in SM] [46]. This finding is in sharp contrast to the case of KV_3Sb_5 , in which both the CDW induced energy gap around M and band folding can be well identified, as illustrated in Fig. 5(b). As for V-based kagome metals, the origin of CDW is closely related to the Fermi surface instability caused by nesting between neighbouring VHSs around E_F and the softening of phonons. However, VHSs in ATi_3Bi_5 are located well above E_F [right panel of Fig. 5(a)], and thus the nesting induced Fermi surface instability is absent. It might account for the missing of CDW transition in Ti-based kagome metals. To better understand the formation of CDW in kagome metals, we first estimated the zero-frequency joint DOSs contributed by the experimentally determined Fermi surfaces for both kagome systems [see details in SM [46]], which describe the phase spaces for electron scatterings from states at \mathbf{k} to those at $\mathbf{k} + \mathbf{q}$ at the Fermi surface. In contrast to KV_3Sb_5 [Fig. 5(d)], where the resulting Joint DOS exhibits peaks at the CDW wave vectors \mathbf{q}_i ($i=1, 2$ and 3),

there exist no peaks appearing at the specific wave vector for RbTi_3Bi_5 , as shown in Fig. 5(c), suggesting the absence of charge-ordering instabilities therein. Furthermore, we calculated phonon dispersions along high-symmetry paths, as shown in Figs. 5(e) and 5(f) for RbTi_3Bi_5 and KV_3Sb_5 , respectively. Distinct from the case of KV_3Sb_5 , the phonon dispersion of RbTi_3Bi_5 is free of imaginary phonons and shows rather stable structure, which further eliminates the possibility of CDW formation in this material.

Recently, two scanning tunneling microscopy (STM) groups reported the electronic nematic phase existing in ATi_3Bi_5 with the rotation symmetry breaking, which occurs in the absence of the concomitant translation symmetry breaking induced by CDW [48, 49]. Although our ARPES results cannot directly reveal the directionality in the low-energy electronic structure at the first sight, the autocorrelation of ARPES spectra, which has been applied to give a reasonable count for charge-ordering instabilities of various compounds [50–54], indeed exhibits evident anisotropy in the amplitudes between the three nominally identical directions. Given that the autocorrelation analysis on ARPES determined Fermi surface would accumulate all subtle inhomogeneity of states, the directionality in resulting autocorrelation might be related to the underlying pure electronic nematic phase. Interestingly, our autocorrelation result on KV_3Sb_5 [Fig. 5(d)] as well illustrates anisotropic amplitudes along three nominally equivalent directions, which is consistent our previous reports [55]. However, we note that the anisotropy in the autocorrelation result can be affected by a variety of factors, such as the matrix element effects, and a conclusive evidence on the nematicity in the electronic structure of ATi_3Bi_5 still needs further confirmation.

In conclusion, we revealed the coexistence of flat bands, type-II DNLs and \mathbb{Z}_2 topological bands in the newly discovered titanium-based kagome metals. We then investigated the underlying mechanism of vanishing CDW states in ATi_3Bi_5 by comparing to KV_3Sb_5 side-by-side, and confirmed that VHSs around E_F play the key role in forming CDW in kagome metals. We also discovered that RbTi_3Bi_5 shows similar rotation symmetry breaking to KV_3Sb_5 , implying the possible hidden nematic phase without the intertwined CDW in ATi_3Bi_5 . Our findings thus provided important insights into non-trivial band topology and nematic order in titanium-based kagome metals.

We acknowledge the support by the National Natural Science Foundation of China (Grants No. U2032208, 92065201, 12222413, 12004405 and 12174257), the Shanghai Science and Technology Innovation Action Plan (Grant No. 21JC1402000), the Natural Science Foundation of Shanghai (Grant No. 22ZR1473300) and the National Key R & D program of China (Grant No. 2020YFA0309601). Y. F. Guo was sponsored by Double First-Class Initiative Fund of ShanghaiTech University. Part of this research used Beamline 03U of the Shanghai Synchrotron Radiation Facility, which is supported by ME² project under Contract No. 11227902 from National Natural Science Foundation of China.

- [1] L. Ye, M. Kang, J. Liu, F. Von Cube, C. R. Wicker, T. Suzuki, C. Jozwiak, A. Bostwick, E. Rotenberg, D. C. Bell, *et al.*, *Nature* **555**, 638 (2018).
- [2] J.-X. Yin, S. S. Zhang, H. Li, K. Jiang, G. Chang, B. Zhang, B. Lian, C. Xiang, I. Belopolski, H. Zheng, *et al.*, *Nature* **562**, 91 (2018).
- [3] Z. Liu, M. Li, Q. Wang, G. Wang, C. Wen, K. Jiang, X. Lu, S. Yan, Y. Huang, D. Shen, *et al.*, *Nature communications* **11**, 1 (2020).
- [4] N. Morali, R. Batabyal, P. K. Nag, E. Liu, Q. Xu, Y. Sun, B. Yan, C. Felser, N. Avraham, and H. Beidenkopf, *Science* **365**, 1286 (2019).
- [5] D. Liu, A. Liang, E. Liu, Q. Xu, Y. Li, C. Chen, D. Pei, W. Shi, S. Mo, P. Dudin, *et al.*, *Science* **365**, 1282 (2019).
- [6] J.-X. Yin, S. S. Zhang, G. Chang, Q. Wang, S. S. Tsirkin, Z. Guguchia, B. Lian, H. Zhou, K. Jiang, I. Belopolski, *et al.*, *Nature Physics* **15**, 443 (2019).
- [7] Y. Xing, J. Shen, H. Chen, L. Huang, Y. Gao, Q. Zheng, Y.-Y. Zhang, G. Li, B. Hu, G. Qian, *et al.*, *Nature communications* **11**, 1 (2020).
- [8] M. Kang, L. Ye, S. Fang, J.-S. You, A. Levitan, M. Han, J. I. Facio, C. Jozwiak, A. Bostwick, E. Rotenberg, *et al.*, *Nature materials* **19**, 163 (2020).
- [9] X. Teng, L. Chen, F. Ye, E. Rosenberg, Z. Liu, J.-X. Yin, Y.-X. Jiang, J. S. Oh, M. Z. Hasan, K. J. Neubauer, *et al.*, *Nature* **609**, 490 (2022).
- [10] S. Yan, D. A. Huse, and S. R. White, *Science* **332**, 1173 (2011).
- [11] T.-H. Han, J. S. Helton, S. Chu, D. G. Nocera, J. A. Rodriguez-Rivera, C. Broholm, and Y. S. Lee, *Nature* **492**, 406 (2012).
- [12] J. Helton, K. Matan, M. Shores, E. Nytko, B. Bartlett, Y. Yoshida, Y. Takano, A. Suslov, Y. Qiu, J.-H. Chung, *et al.*, *Physical review letters* **98**, 107204 (2007).
- [13] E. Tang, J.-W. Mei, and X.-G. Wen, *Physical review letters* **106**, 236802 (2011).
- [14] E. J. Bergholtz, Z. Liu, M. Trescher, R. Moessner, and M. Udagawa, *Physical review letters* **114**, 016806 (2015).
- [15] B. R. Ortiz, S. M. Teicher, Y. Hu, J. L. Zuo, P. M. Sarte, E. C. Schueller, A. M. Abeykoon, M. J. Krogstad, S. Rosenkranz, R. Osborn, *et al.*, *Physical Review Letters* **125**, 247002 (2020).
- [16] T. Neupert, L. Santos, C. Chamon, and C. Mudry, *Physical review letters* **106**, 236804 (2011).
- [17] D. Grohol, K. Matan, J.-H. Cho, S.-H. Lee, J. W. Lynn, D. G. Nocera, and Y. S. Lee, *Nature materials* **4**, 323 (2005).
- [18] E. Liu, Y. Sun, N. Kumar, L. Muechler, A. Sun, L. Jiao, S.-Y. Yang, D. Liu, A. Liang, Q. Xu, *et al.*, *Nature physics* **14**, 1125 (2018).
- [19] Y.-X. Jiang, J.-X. Yin, M. M. Denner, N. Shumiya, B. R. Ortiz, G. Xu, Z. Guguchia, J. He, M. S. Hossain, X. Liu, *et al.*, *Nature Materials* **20**, 1353 (2021).
- [20] H.-C. Jiang, Z.-Y. Weng, and D. N. Sheng, *Physical Review Letters* **101**, 117203 (2008).
- [21] Y. Hu, S. M. Teicher, B. R. Ortiz, Y. Luo, S. Peng, L. Huai, J. Ma, N. C. Plumb, S. D. Wilson, J. He, *et al.*, *Science Bulletin* **67**, 495 (2022).
- [22] K. Chen, N. Wang, Q. Yin, Y. Gu, K. Jiang, Z. Tu, C. Gong, Y. Uwatoko, J. Sun, H. Lei, *et al.*, *Physical Review Letters* **126**, 247001 (2021).
- [23] Z. Liang, X. Hou, F. Zhang, W. Ma, P. Wu, Z. Zhang, F. Yu, J.-J. Ying, K. Jiang, L. Shan, *et al.*, *Physical Review X* **11**, 031026 (2021).
- [24] H.-S. Xu, Y.-J. Yan, R. Yin, W. Xia, S. Fang, Z. Chen, Y. Li, W. Yang, Y. Guo, and D.-L. Feng, *Physical Review Letters* **127**, 187004 (2021).
- [25] R. Lou, A. Fedorov, Q. Yin, A. Kuibarov, Z. Tu, C. Gong, E. F. Schwier, B. Büchner, H. Lei, and S. Borisenko, *Physical Review Letters* **128**, 036402 (2022).
- [26] H. Chen, H. Yang, B. Hu, Z. Zhao, J. Yuan, Y. Xing, G. Qian, Z. Huang, G. Li, Y. Ye, *et al.*, *Nature* **599**, 222 (2021).
- [27] B. R. Ortiz, L. C. Gomes, J. R. Morey, M. Winiarski, M. Bordelon, J. S. Mangum, I. W. Oswald, J. A. Rodriguez-Rivera, J. R. Neilson, S. D. Wilson, *et al.*, *Physical Review Materials* **3**, 094407 (2019).
- [28] H. Zhao, H. Li, B. R. Ortiz, S. M. Teicher, T. Park, M. Ye, Z. Wang, L. Balents, S. D. Wilson, and I. Zeljkovic, *Nature* **599**, 216 (2021).
- [29] L. Nie, K. Sun, W. Ma, D. Song, L. Zheng, Z. Liang, P. Wu, F. Yu, J. Li, M. Shan, *et al.*, *Nature* **604**, 59 (2022).
- [30] C. Mielke, D. Das, J.-X. Yin, H. Liu, R. Gupta, Y.-X. Jiang, M. Medarde, X. Wu, H. Lei, J. Chang, *et al.*, *Nature* **602**, 245 (2022).
- [31] C. Guo, C. Putzke, S. Konyzheva, X. Huang, M. Gutierrez-Amigo, I. Errea, D. Chen, M. G. Vergniory, C. Felser, M. H. Fischer, *et al.*, *Nature* , 1 (2022).
- [32] Y. Xu, Z. Ni, Y. Liu, B. R. Ortiz, Q. Deng, S. D. Wilson, B. Yan, L. Balents, and L. Wu, *Nature Physics* , 1 (2022).
- [33] T. Neupert, M. M. Denner, J.-X. Yin, R. Thomale, and M. Z. Hasan, *Nature Physics* **18**, 137 (2022).
- [34] H. Li, H. Zhao, B. R. Ortiz, T. Park, M. Ye, L. Balents, Z. Wang, S. D. Wilson, and I. Zeljkovic, *Nature Physics* **18**, 265 (2022).
- [35] M. Kang, S. Fang, J.-K. Kim, B. R. Ortiz, S. H. Ryu, J. Kim, J. Yoo, G. Sangiovanni, D. Di Sante, B.-G. Park, *et al.*, *Nature Physics* **18**, 301 (2022).
- [36] M. Kang, S. Fang, J. Yoo, B. R. Ortiz, Y. M. Oey, J. Choi, S. H. Ryu, J. Kim, C. Jozwiak, A. Bostwick, *et al.*, *Nature Materials* , 1 (2022).
- [37] M. Hastings, *Physical Review B* **63**, 014413 (2000).
- [38] I. Mazin, H. O. Jeschke, F. Lechermann, H. Lee, M. Fink, R. Thomale, and R. Valentí, *Nature communications* **5**, 1 (2014).
- [39] H. Yang, Z. Zhao, X.-W. Yi, J. Liu, J.-Y. You, Y. Zhang, H. Guo, X. Lin, C. Shen, H. Chen, *et al.*, *arXiv preprint arXiv:2209.03840* (2022).
- [40] D. Werhahn, B. R. Ortiz, A. K. Hay, S. D. Wilson, R. Seshadri, and D. Johrendt, *Zeitschrift für Naturforschung B* (2022).
- [41] H. Yang, Z. Huang, Y. Zhang, Z. Zhao, J. Shi, H. Luo, L. Zhao, G. Qian, H. Tan, B. Hu, *et al.*, *Science Bulletin* (2022).
- [42] Y. Li, Q. Li, X. Fan, J. Liu, Q. Feng, M. Liu, C. Wang, J.-X. Yin, J. Duan, X. Li, *et al.*, *Physical Review B* **105**, L180507 (2022).
- [43] T. Kato, Y. Li, K. Nakayama, Z. Wang, S. Souma, F. Matsui, M. Kitamura, K. Horiba, H. Kumigashira, T. Takahashi, Y. Yao, and T. Sato, *Phys. Rev. Lett.* **129**, 206402 (2022).
- [44] Y. Jiang, Z. Yu, Y. Wang, T. Lu, S. Meng, K. Jiang, and M. Liu, *Chinese Physics Letters* **39**, 047402 (2022).
- [45] X.-W. Yi, X.-Y. Ma, Z. Zhang, Z.-W. Liao, J.-Y. You, and G. Su, *arXiv preprint arXiv:2202.05588* (2022).
- [46] See Supplemental Material at for details of methods (Single crystal synthesis and characterization, ARPES and calculations, which includes Refs. [56–61]).
- [47] L. Fu and C. L. Kane, *Physical Review B* **74**, 195312 (2006).
- [48] H. Yang, Y. Ye, Z. Zhao, J. Liu, X.-W. Yi, Y. Zhang, J. Shi, J.-Y. You, Z. Huang, B. Wang, *et al.*, *arXiv preprint*

- arXiv:2211.12264 (2022).
- [49] H. Li, S. Cheng, B. R. Ortiz, H. Tan, D. Werhahn, K. Zeng, D. Jorhendt, B. Yan, Z. Wang, S. D. Wilson, *et al.*, arXiv preprint arXiv:2211.16477 (2022).
- [50] D. Shen, B. Xie, J. Zhao, L. Yang, L. Fang, J. Shi, R. He, D. Lu, H. Wen, and D. Feng, *Physical review letters* **99**, 216404 (2007).
- [51] U. Chatterjee, M. Shi, A. Kaminski, A. Kanigel, H. Fretwell, K. Terashima, T. Takahashi, S. Rosenkranz, Z. Li, H. Raffy, *et al.*, *Physical review letters* **96**, 107006 (2006).
- [52] K. McElroy, G.-H. Gweon, S. Zhou, J. Graf, S. Uchida, H. Eisaki, H. Takagi, T. Sasagawa, D.-H. Lee, and A. Lanzara, *Physical review letters* **96**, 067005 (2006).
- [53] D. Shen, Y. Zhang, L. Yang, J. Wei, H. Ou, J. Dong, B. Xie, C. He, J. Zhao, B. Zhou, *et al.*, *Physical review letters* **101**, 226406 (2008).
- [54] S. Cho, H. Ma, W. Xia, Y. Yang, Z. Liu, Z. Huang, Z. Jiang, X. Lu, J. Liu, Z. Liu, *et al.*, *Physical Review Letters* **127**, 236401 (2021).
- [55] Z. Jiang, H. Ma, W. Xia, Q. Xiao, Z. Liu, Z. Liu, Y. Yang, J. Ding, Z. Huang, J. Liu, *et al.*, arXiv preprint arXiv:2208.01499 (2022).
- [56] Y.-C. Yang, Z.-T. Liu, J.-S. Liu, Z.-H. Liu, W.-L. Liu, X.-L. Lu, H.-P. Mei, A. Li, M. Ye, S. Qiao, *et al.*, *Nuclear Science and Techniques* **32**, 1 (2021).
- [57] Z. Sun, Z. Liu, Z. Liu, W. Liu, F. Zhang, D. Shen, M. Ye, and S. Qiao, *Journal of Synchrotron Radiation* **27**, 1388 (2020).
- [58] G. Kresse and J. Furthmüller, *Phys. Rev. B* **54**, 11169 (1996).
- [59] J. P. Perdew, K. Burke, and M. Ernzerhof, *Phys. Rev. Lett.* **77**, 3865 (1996).
- [60] A. A. Mostofi, J. R. Yates, Y.-S. Lee, I. Souza, D. Vanderbilt, and N. Marzari, *Computer physics communications* **178**, 685 (2008).
- [61] M. L. Sancho, J. L. Sancho, J. L. Sancho, and J. Rubio, *Journal of Physics F: Metal Physics* **15**, 851 (1985).